Seismotectonics of the Bitlis–Zagros Fold and Thrust Belt in Northern Iraq and Surrounding Regions from Moment Tensor Analysis

Wathiq Abdulnaby, Hanan Mahdi, Nazar M. S. Numan & Haydar Al-Shukri

Pure and Applied Geophysics
pageoph

ISSN 0033-4553

Pure Appl. Geophys.
DOI 10.1007/s00024-013-0688-4

Springer

Pure Appl. Geophys.
© 2013 Springer Basel
DOI 10.1007/s00024-013-0688-4

Pure and Applied Geophysics

Seismotectonics of the Bitlis–Zagros Fold and Thrust Belt in Northern Iraq and Surrounding Regions from Moment Tensor Analysis

WATHIQ ABDULNABY,[1] HANAN MAHDI,[2] NAZAR M. S. NUMAN,[3] and HAYDAR AL-SHUKRI[4]

Abstract—Northern Iraq represents part of the convergent plate boundary between the Arabian and Eurasian plates. The collision zone between these two plates is manifested by the Bitlis–Zagros Fold and Thrust Belt. This belt is one of the most seismically active regions among the present active belts. This study intends to improve our knowledge on the seismotectonic activities in northern Iraq and the surrounding areas. To reach this goal, we used the waveform moment tensor inversion method to determine the focal depths, moment magnitudes, fault plane solutions, and directions of the principal stress axes of 25 events with magnitudes ≥3.5. The seismic data of these events were collected from 54 broadband stations which belong to the Kandilli Observatory and Earthquake Research Institute, the Incorporated Research Institutions for Seismology, the Observatories and Research Facilities for European Seismology, and the Iraqi Seismological Network. Computer Programs in Seismology, version 3.30 (HERRMANN and AMMON 2004), was used for analysis. The results show that the focal depth of these events ranged from 15 to 25 km in general. The fault plane solutions show that the strike-slip mechanism is the most dominant mechanism in the study area, usually with a reverse component. The stress regime shows three major directions; north–south, northeast-southwest, and east–west. These directions are comparable with the tectonic regime in the region.

1. Introduction

Northern Iraq represents part of the convergent plate boundary between the Arabian and Eurasian plates (Fig. 1). The Eurasian plate consists of two plates, namely, the Anatolian and Iranian plates in the north and northeast of the studied region, consecutively. The collision between these plates began after the closure of the Neo-Tethys Ocean in the Miocene. This collision continues to the present day (e.g. DEWEY *et al*. 1973; NUMAN 1997). The collision has resulted in the formation of the Bitlis–Zagros Fold and Thrust Belt that extends from Turkey and Iraq in the north to the Strait of Hormuz in the south. Geological evidence indicates that the Bitlis–Zagros Fold and Thrust Belt underwent various tectonic episodes that affected different parts of the belt (FALCON 1974; STOCKLIN 1968). The Bitlis–Zagros Fold and Thrust Belt is one of the most seismically active regions among the present active belts (TATAR *et al*. 2004).

This study intends to improve our knowledge on the seismic activities in northern Iraq and the surrounding areas. To reach this goal, we used seismic data from 54 seismic stations to estimate the focal depths, moment magnitudes, fault plane solutions, and directions of the principal stress axes of 25 events. We have tried to infer the prevailing mechanism of the fault displacements and the stress regime in the study area. Another goal of this study has been to provide a regional velocity model and pre-computed Green's functions that can be used accurately to determine the moment tensor in the Bitlis–Zagros Fold and Thrust Belt in northern Iraq and the surrounding regions.

2. Tectonic and Structural Setting

The Bitlis–Zagros Fold and Thrust Belt has two distinct trends, NW–SE (here called the Zagros Trend) between the Arabian and Iranian plates, and E–W (called the Bitlis Trend) between the Arabian

[1] Geology Department, College of Science, University of Basra, Basra, Iraq. E-mail: wathiq1972@yahoo.com
[2] Graduate Institute of Technology (GIT), University of Arkansas at Little Rock, 2801 South University Ave, Little Rock, AR 72204, USA. E-mail: hhmahdi@ualr.edu
[3] Engineering and Applied Science, University of Duhok, Duhok, Iraq. E-mail: nazarnuman@yahoo.com
[4] Department of Applied Science, University of Arkansas at Little Rock, 2801 South University Ave, Little Rock, AR 72204, USA. E-mail: hjalshukri@ualr.edu

Published online: 29 June 2013

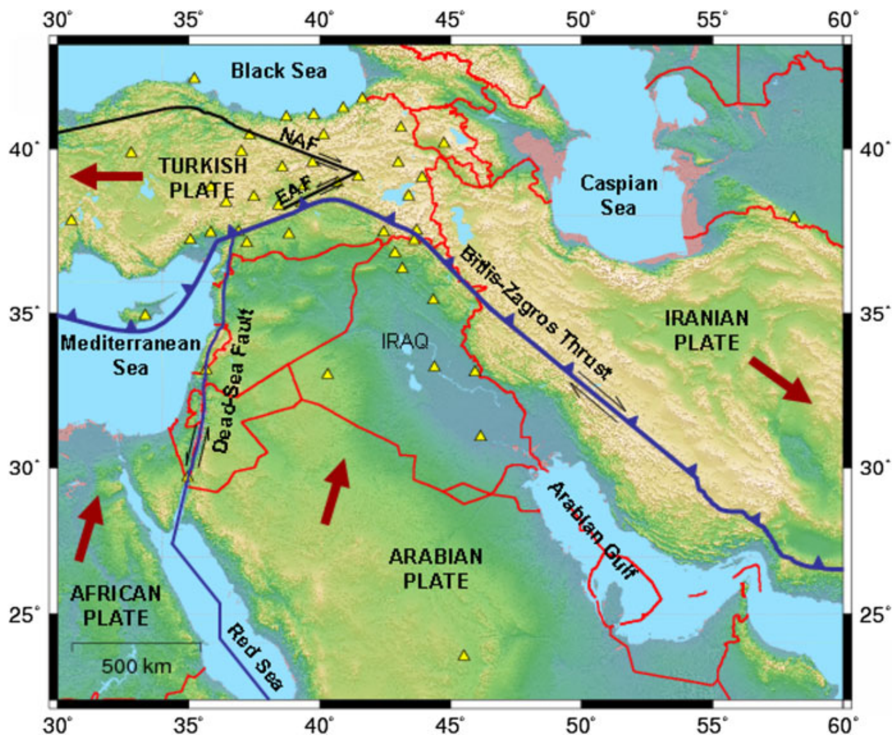

Figure 1
Tectonic map of the study area. *Yellow triangles* represent the location of the stations that were selected for source mechanism studies

and Anatolian plates (Fig. 1). The curved nature of the trend of this mountain belt is being dictated by the curvature of the northern Arabian Plate margin.

The collision of the Arabian Plate with the Anatolian Plate has initiated a space problem for the Anatolian Plate. As a result the Turkish Plate is moving laterally to the west along two major conjugate strike-slip faults which cut through rock to the surface. These are the East Anatolian Fault (EAF) and North Anatolian Fault (NAF) which are responsible for triggering some of the most devastating earthquakes in Turkey (Fig. 1). This phenomenon is called the "westward tectonic escape of Turkey" as described by Sengor *et al*. (1985) and Elitok and Dolmaz (2011).

Figure 2 shows the tripartite division of the Iraqi geology according to Numan *et al*. (1998). These divisions from northeast to southwest are: the Thrust Zone (1), the Foreland Fold Belt (2), and the Arabian Platform (3). The Foreland Fold Belts consists of three subdivision zones. They are, from northeast to southwest: Imbrication Zone (2A), Highly Folded Zone (2B), and Foothill Zone (2C) (Numan 1997, 2000). The Thrust Zone represents subductional tectonic facies of the Zagros Thrust (Numan 1997). Our study area located within of the Thrust Zone and the Foreland Fold Belt.

In northern Iraq, Numan (1997) described a set of listric normal faults in the basement rocks beneath the sedimentary cover. These faults were tensional normal faults which resulted from the opening of the Neo-Tethys Ocean in the Early Triassic. The fault planes (dipping mostly to the north and northeast) are steep in shallow depths and curve to a subhorizontal attitude deep into the crystalline basement. The closure of the Neo-Tethys Ocean and subsequent continental plate collision created a compressional environment which leads to reversal of movement on the originally normal listric faults, sedimentary basin inversion, and the shaping and tightening of folds in the Foreland Folds Belt. This scenario continues to the present day according Numan (1997, 2001).

The folds of the Foreland Fold Belt of Iraq have two trends: the Bitlis trend (east–west) and the Zagros

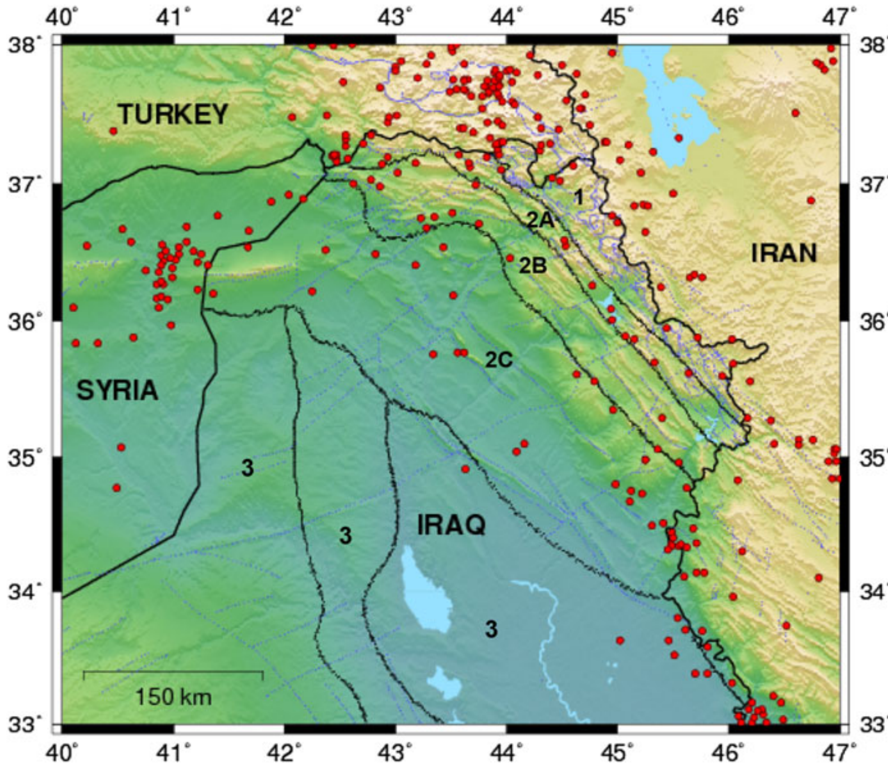

Figure 2
The tectonic division of northern Iraq modified from Numan (1997, 2000) and Numan *et al.* (1998). *Solid black curvy lines* represent the tectonic boundary between different tectonic sub-regions. *1* Thrust zone, *2A* imrication zone, *2B* highly folded zone, *2C* foothill zone, and *3* Arabian platform. *2A*, *2B*, and *2C* called Foreland Fold Belt. The *red dots* represent 297 earthquakes with magnitude ≥3.5 occurred in the study area for the period from October 2004 to October 2012 (EMSC catalog)

trend (northwest–southeast). These folds are generally asymmetrical, and they are either simple buckle folds or fault-related folds. The fault-related folds are associated with basement reactivation which heralded reverse displacements on the originally normal listric faults as well as strike-slip faults or wrench tectonics between basement blocks, (Numan 1984, 2000; Numan and Al-Azzawi 1993). The listric faults are parallel to the axes of anticlines.

3. Crustal Structure

Previous geophysical studies of the crustal structure of northern Iraq and adjacent areas indicate that the Moho depth ranges from 40 to 60 km and the depth of Conrad discontinuity from 18 to 22 km. Table 1 and Fig. 3 show the crustal thickness of the study area beneath 19 stations according to Gök *et al.* (2007, 2008, 2011), Mellors *et al.* (2008), Gritto *et al.* (2008), Afsari *et al.* (2011), and Abdulnaby *et al.* (2012). Gök *et al.* (2008) suggest that the crystalline crust across the northern Arabian Platform is uniform. Therefore, the variation of crustal thickness in the Fold-Thrust Belt and Foreland Folds Belt reveal the tectonic evolution (further deposition, deformation and crustal shortening) of the collision zone between Arabian and Eurasian plates. Gök *et al.* (2011) reported that the deepest Moho is observed in the Lesser Caucasus region and the shallowest is in Arabian Plate. Afsari *et al.* (2011) found that the area northwest of Zagros and Central Iran has a relatively flat Moho at 40–43 km depth, but there are some exceptions. A local overthrusting system, including a dipping Moho boundary, was their alternative explanation for these exceptions. One of these exceptions is located in the central part of the Kermanshah region, beneath station VIS, that has a significant crustal thickness that

Table 1

The crustal thickness (Moho depth) within and around the northwestern margin of the Arabian plate in Iraq

Country	Code	Latitude	Longitude	Elv. (m)	Moho (km)	Sources
Iran	DHR	34.6997	46.3860	1,434	42	Afsari *et al.* (2011)
	GHG	34.3294	46.5686	2,090	46	
	KOM	34.1764	47.5144	1,502	42	
	LIN	34.9186	46.9624	2,195	42	
	VIS	34.5253	46.8527	1,135	50	
Turkey	CUKT	37.2473	43.6077	1,300	46	Mellors *et al.* (2008)
	SEMD	37.5000	44.5000	–	44	
	SIRT	37.5010	42.4392	1,040	46	
	MRDN	37.9000	40.5000	–	40	Gök *et al.* (2007)
Iraq	KSBB	35.0415	45.7092	550	49	Gritto *et al.* (2008)
	KSSS	35.7696	46.2362	1,515	52	
	KSWW	36.1493	45.2624	1,310	54	
	KSJS	35.4965	45.3452	825	49	
	KEHH	36.6764	45.0470	1,725	50	
	KESM	36.9846	44.1981	1,000	39	
	KDDA	37.2125	42.8207	750	52	
	KEKZ	35.9893	44.0970	450	45	
	MSL	36.3817	43.1483	242	42	Gök *et al.* (2008)
	DHK	36.8606	42.8665	766	42	Abdulnaby *et al.* (2012)

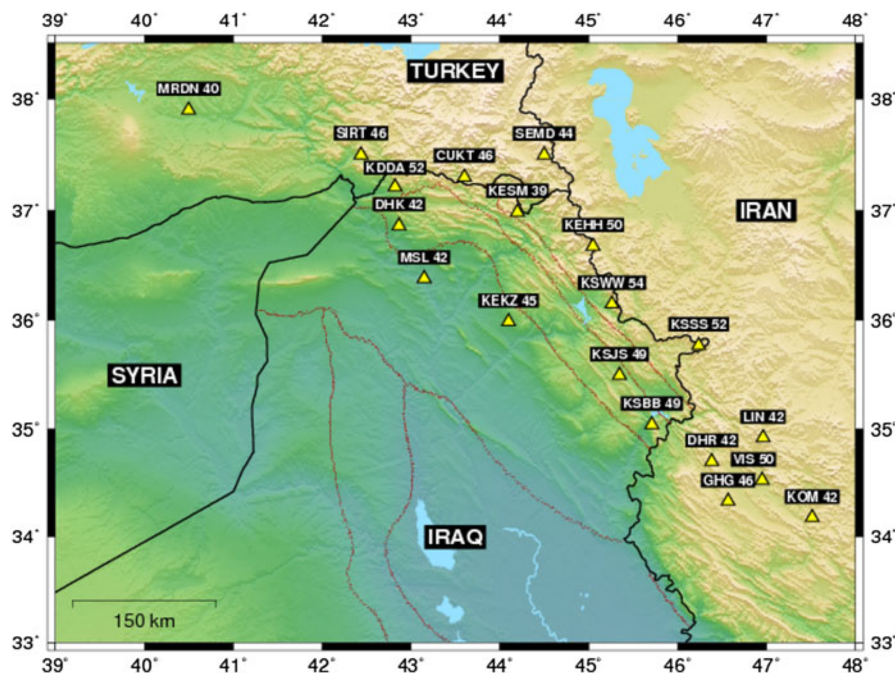

Figure 3
Crustal thickness (Moho depths in kilometers) beneath 19 seismic stations (*yellow triangles*) based on Table 1

reaches to approximately 50 km. In general, the average of Moho depth beneath the Northwest Zagros area is about 42 km increasing toward the Sanandaj–Sirjan Metamorphic Zone and reaches 51 km, where the two crusts (Zagros and Central Iran) are assumed to be superposed (Afsari *et al.* 2011).

4. Seismicity

In the Zagros collision zone, the seismicity rates are among the highest in the world for a fold and thrust belt (Tatar *et al*. 2004). Few studies of source analysis using first motion techniques have been done in the Thrust Zone and Foreland Fold Belt (Kim and Nuttli 1977; Fahmi *et al*. 1986; Al-Heety 1997; Alsinawi and Al-Heety 1997). These studies reported a strike-slip mechanism with reverse component (Fahmi *et al*. 1986), and NE and NW trending reverse faulting (Kim and Nuttli 1977; Al-Heety 1997; Alsinawi and Al-Heety 1997). According to Engdahl *et al.* (2006), most of the earthquakes in the Zagros fold-and-thrust region are shallower than 30 km, and the seismicity in the southeast Anatolian thrust zone shows moderate magnitude earthquakes with focal depth ranging from 10 to 20 km and is dominated by the strike-slip focal mechanism.

According to the European Mediterranean Seismologic Center (EMSC) catalog, about 1,000 events have been recorded in northern Iraq (latitude 34°N to 38°N and longitude 40°E to 47°E) during the last 8 years (October 1, 2004, to October 1, 2012). These events have magnitudes ranging between two to six and a depth of less than 40 km in general. Figure 2 shows 297 earthquakes with magnitude ≥3.5 occurred in the study area according to the EMSC catalog for the period from October 2004 to October 2012.

5. Datasets

Seismic data of 25 events with magnitudes ≥3.5 were collected from 54 broadband stations that belong to the Kandilli Observatory and Earthquake Research Institute (KOERI), the Incorporated Research Institutions for Seismology (IRIS), the Observatories and Research Facilities for European Seismology (ORFUES), and the Iraqi Seismological Network (ISN). Also, the Duhok station, which is operated by the University of Arkansas at Little Rock (UALR) Earthquake Center, was used (see Table 2). The epicentral distances between the stations and seismic events ranged from 10 to 2,000 km (Fig. 1). These data were collected to determine the focal depths, moment magnitudes, fault plane solutions, and directions of principal stress axes. The source parameters of the seismic events were selected from the EMSC seismic catalog. The accuracy of the locations, depths, and magnitudes is a critical factor for reliably identifying fault plane solutions.

6. Methodology

There are many methods that can be used to determine the fault plane solution (or the focal mechanism solution "FMS"). In this study, the regional moment tensor inversion method was implemented to estimate the focal depths, moment magnitudes, fault plane solutions, and directions of principal stress axes of 25 events with magnitudes ≥3.5. A package of programs named Computer Programs in Seismology (CPS), version 3.30, developed by Herrmann and Ammon (2004) was used to conduct the moment tensor inversion and calculate the Green's functions.

If the earth's structure is known and waveform data are available, the seismic moment tensor and also the focal mechanism of an earthquake can be calculated by inversion, which can be done from amplitude ratios or full waveform data (Shearer 2009; Havskov and Ottemöller 2010). Generally, the quality of the moment tensor inversion depends on the number of data available and the azimuthal distribution of stations around the source (Kayal 2008). The most advanced methods of moment tensor inversion use complete seismograms including *P*, *S*, and surface waves. These advanced methods use earthquakes which have magnitudes that equal or exceed three, because the seismograms of earthquakes with magnitude smaller than three cannot be realistically modeled.

There are two techniques for source inversion; these are surface-wave radiation patterns and full waveform inversion. In this study, we used the waveform inversion (grid search) technique. Searching over all possible focal mechanisms is used in this technique. In general, the requirements of performing the moment tensor inversion are: waveform data, instrument response, station locations, earthquake location, velocity model, and Green's functions.

Table 2

Seismic stations used in this study

Station ID	Network	Latitude	Longitude	Station ID	Network	Latitude	Longitude
ABKT	II	37.9304	58.1189	KARA	KO	37.2607	35.0547
AGRB	KO	39.5755	42.9920	KARS	KO	40.6152	43.0937
ANTO	IU	39.8680	32.7934	KIEV	IU	50.7012	29.2242
APE	GI	37.0689	25.5306	KIV	II	43.9553	42.6863
BAYT	KO	40.3935	40.1410	KMRS	KO	37.5053	36.9000
BCA	KO	41.4450	41.6223	KOZT	KO	37.4805	35.8268
BHD	ISN	33.2743	44.3858	KSDI	GE	33.1920	35.6590
BNGB	KO	38.9913	40.6792	KTUK	KO	40.9870	39.7667
BNN	KO	38.8522	35.8472	MALT	GE	38.3134	38.4273
CLDR	KO	39.1440	43.9172	MSL	ISN	36.3816	43.1483
CSS	GE	34.911	33.3310	NSR	ISN	31.0100	46.1400
CUKT	KO	37.2473	43.6077	PLD	BS	42.1049	24.7031
DARE	KO	38.5712	37.4832	PTK	KO	38.8923	39.3923
DHK	–	36.8606	42.8665	PZAR	KO	41.1780	40.8988
EIL	GE	29.6699	34.9512	RAYN	II	23.5225	45.5032
ERZN	KOI	39.5867	39.7220	RSDY	KO	40.3972	37.3273
ESPY	KO	40.9167	38.7273	RTB	ISN	33.0295	40.3077
GAZ	KO	37.1722	37.2113	SANT	GE	36.371	25.4590
GNI	IU	40.1480	44.7410	SARI	KO	38.4072	36.4182
GVD	GE	34.8392	24.0873	SIRT	KO	37.5010	42.4392
HAKT	TU	37.5579	43.7071	SNOP	KO	42.0195	35.2068
IBDR	ISN	33.1100	45.9300	SVRC	KO	38.3775	39.3060
IDI	MN	35.2880	24.8900	SVSK	KO	39.9175	36.9925
IKRK	ISN	35.4000	44.3400	TIRR	GE	44.4581	28.4128
ILIC	KO	39.4520	38.5678	URFA	KO	37.4410	38.8213
ISP	GE	37.8433	30.5093	VANB	KO	38.5950	43.3888
JMB	BS	42.4667	26.5833	VRTB	KO	39.1603	41.4560

7. Green's Functions

A theoretical seismogram must be generated in order to do moment tensor inversion using complete seismograms. This can be done with different methods, and each method has its own advantages and disadvantages (Shearer 2009). In this study, Green's function for the northern Iraq region was computed by using the CPS package based on the flat velocity model which was modified from Alsinawi and Al-Heety 1994; Mooney *et al*. 1998; Abdulnaby *et al*., 2012 (Table 3). In this velocity model, we have taken into account all of the elastic properties of the material and the appropriate boundary conditions, because using an appropriate regional velocity model is important to match the waveforms and also to define the moment magnitude of the earthquake (Herrmann *et al*. 2011).

Table 3

Velocity model used to build Green's functions of the study area (modified from Alsinawi and Al-Heety 1994; Mooney et al. 1998; Abdulnaby et al. 2012)

H (km)	VP (km/s)	VS (km/s)	Density (gm/cm^3)
1.90	3.9289	2.1916	2.3104
4.10	5.7546	3.2098	2.6505
10.0	6.6364	3.7019	2.8833
23.0	6.9038	3.8509	2.9542
0.00	7.7111	4.1010	3.2120

To generate Green's functions for the local and regional seismograms, two synthetic seismogram techniques were used: wavenumber integration and modal superposition of surface waves. Wavenumber integration is a homogeneous layer method that needs a velocity model which consists of a series of horizontal layers with constant properties within each layer (Shearer 2009). It is also a complete seismogram synthesis that is restricted to a one dimension velocity model. The computational time for the wavenumber integration code follows the frequency content and the desired distances (Herrmann 2006). Modal superposition of surface waves is an almost complete seismogram synthesis that can be used for low-frequency seismograms. This technique can be much faster than wavenumber integration.

A general inversion of moment tensor requires just ten Green's functions that represent functions of source depth and epicentral distance (Herrmann and Ammon 2003). These ten Green's functions, which are generated by synthetic seismic codes, were combined to create three components for: (1) arbitrarily oriented point forces, (2) double couple sources, and (3) general moment tensor sources. For more details see Herrmann (2006).

For the purpose of result verification, we run moment tensor inversions using the already precalculated Green's functions of Herrmann's for the Western United States (WUS) in addition to our calculated Green's functions. Herrmann (2011) used the WUS model for Turkish events moment tensor analysis. We tested a few of the events using both Green's functions and we found that the results are similar, although our Green's functions model has given a better fit data.

8. *Example of Moment Tensor Inversion*

As an example of the processing of the data, we are showing the event of 2011/12/06 15:46:30 UTC. Data from six stations, which are DHK, IKRK, MSL, SIRT, VANB, and VRTB, with epicentral distance range from 105 to 275 km, were used (Fig. 4). For the

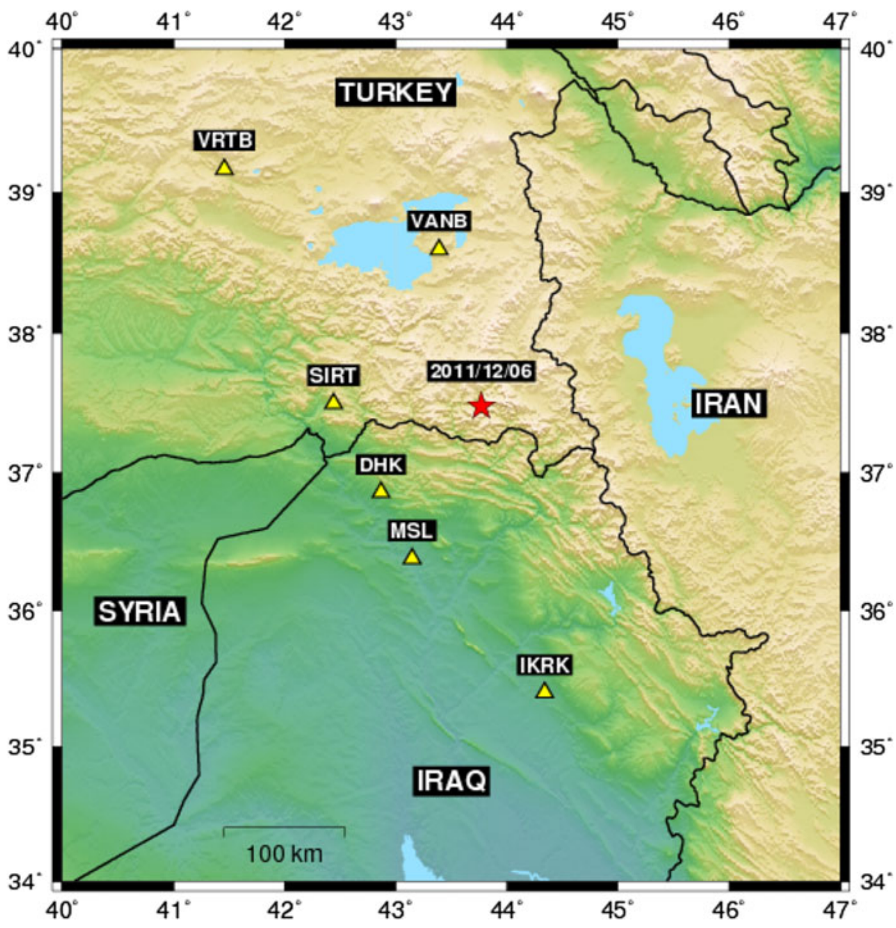

Figure 4
Location (*star*) of the earthquake of 2011/12/06 15:46:30 UTC and the six stations (*yellow triangles*) that were used to estimate the moment tensor inversion

moment inversion of this earthquake we selected four vertical-component (Z), two radial-component (R), and five transverse-component (T) waveforms. Those selected components gave the best fit between observed and predicted waveforms. Figure 5 depicts these 11 observed waveforms (red) with the predicted waveforms (blue). The time shifts indicate the shift of the predicted with respect to the observed traces (Herrmann *et al*. 2011). In our example the low time shift indicates a consistency of the EMSC source location and origin time, as well as the applicability of the velocity model. Figure 6 shows the goodness of the fit as a function of source depth. The maximum limit of the focal depth search is 39 km; and the perfect fit is a value of 1.0. The figure also shows the best mechanisms associated with each source depth. The best fit occurs at a source depth of 15 km. To have a range of acceptable depths for the event, a reasonable threshold with 4 % in the fit parameter was chosen, and then a plus/minus range of depth relative to the depth with highest fit was defined. The result shows that the focal depth of the event was 15 ± 4 km.

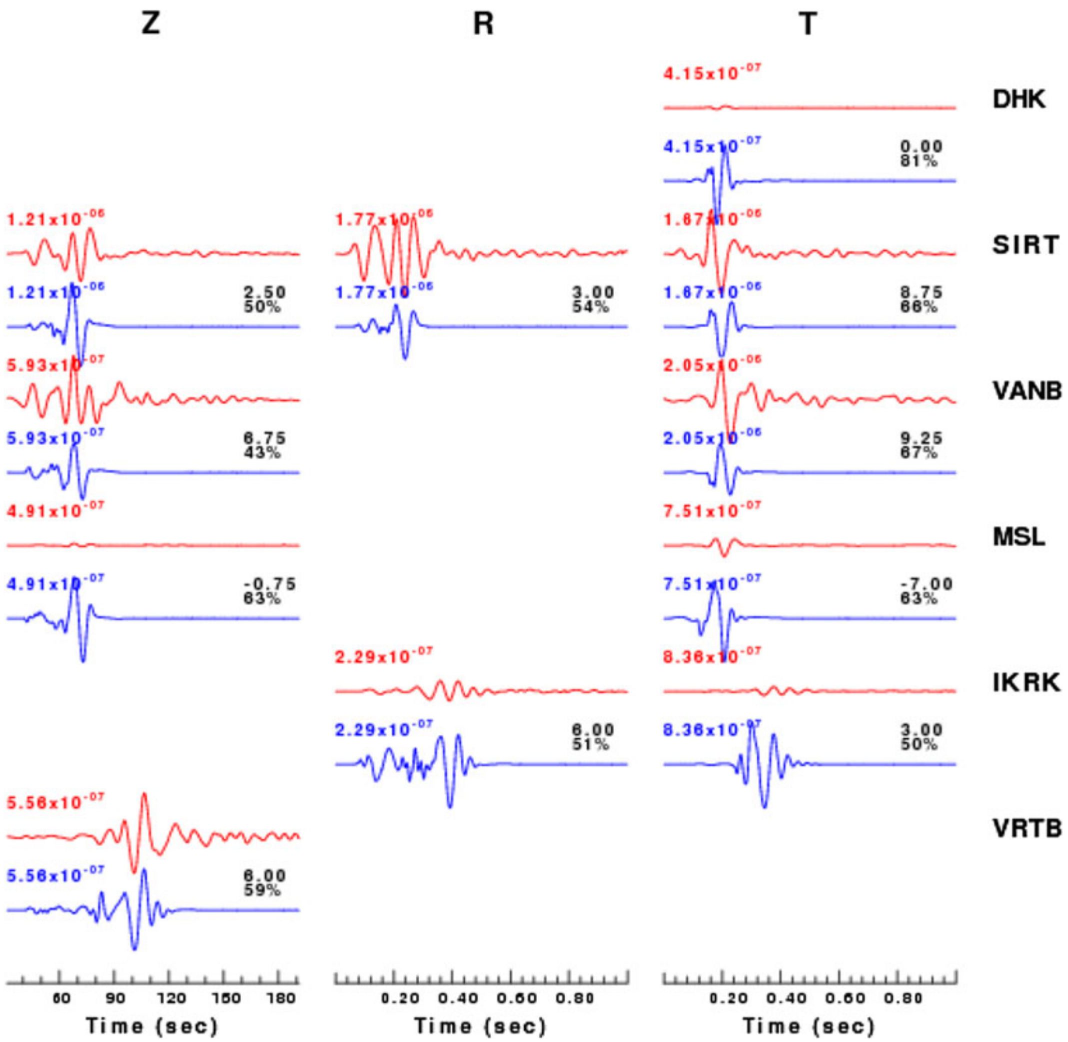

Figure 5
Comparison of observed (*red*) and predicted (*blue*) waveforms for the earthquake of 2011/12/06 15:46:27.7 UTC as a function of absolute travel time. All 11 traces represent ground velocity (m/s) filtered in the 0.02–0.1 Hz band. The peak amplitude is indicated to the left of each trace. The time shift of the synthetic with respect to the observed trace for the best waveform fit is given to the right of each trace in the *top* and the percentage of fit in the *bottom*. The station name is given to the right of the traces

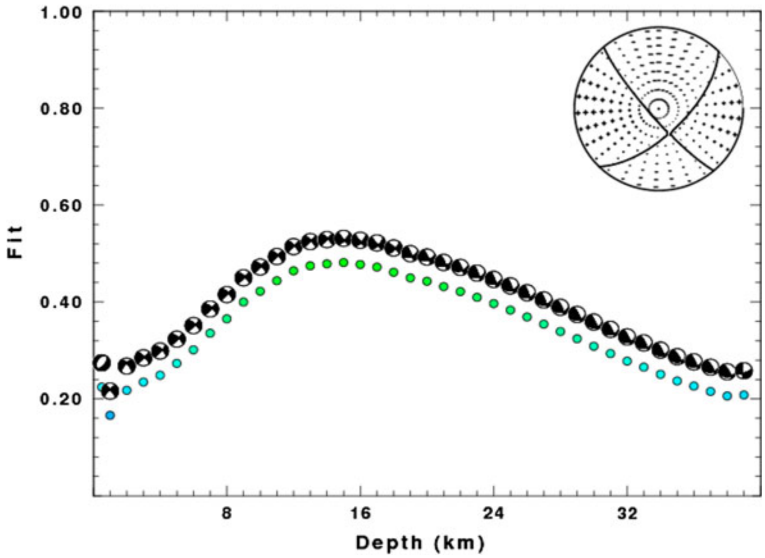

Figure 6
Goodness of the fit as a function of source depth for the earthquake of 2011/12/06 15:46:27.7 UTC. The best fitting mechanism at each source depth is plotted in lower hemisphere projection. The best fit is for a depth of 15 km. The *beach ball* shows the best solution at this depth

9. Results and Discussion

The results of the moment tensor inversion of all events in this study are shown in Table 4. This table also shows the source parameters of the seismic events that were used in this study from the EMSC catalog. The beach balls are plotted on Fig. 7, and the stress vectors are plotted on Fig. 8. In the following sections, we discuss the focal mechanism or the fault plane solutions, the stress vectors, the moment magnitudes, and the focal depths.

9.1. Fault Plane Solutions

From the preferred fault plane solutions, which are shown in Fig. 7, the strike-slip movement mechanism is predominant in the Bitlis trend region. Whereas, the predominant mechanism in the Zagros trend region is the reverse mechanism with slight strike-slip displacements.

9.2. Stress Vectors

For each fault plane solution, the compression (P) axis is located in the center of the dilatational quadrants and at 45° from the nodal plane. The P axis from the fault plane solution is not necessarily correlated with the orientation of the maximum compressive axis (σ_1) (Engelder 1993). However, the average orientation of P axes calculated from a number of fault plane solutions gives a good indication of σ_1 throughout a region. The stress vectors in Fig. 8 show that in the Bitlis–Zagros Fold and Thrust Belt the major compressional directions are: NNE-SSW and NW–SE in the Bitlis trend and NE-SW in the Zagros trend. However, farther south and west the major compressional directions are: WNW-ESE, E-W and ENE-WSW.

9.3. Magnitudes

The reported local magnitudes (M_L) and body wave magnitude (m_b) of the 25 events in this study range from 3.5 to 5.4, while the calculated moment magnitudes (M_W) ranged from 3.32 to 5.66 (see Table 4). For the majority of the events, M_W from moment tensor inversions was less than the reported M_L and m_b. The average difference is 0.28 magnitude units. Kanamori (1983) reported that for events with magnitudes 4 to 6.5, there is a reasonable agreement indicates that the M_L and m_b are equal or more than M_W.

Table 4

Source parameters (EMSC catalog), and focal mechanism solutions of the 25 earthquakes from moment tensor inversion

Number	Date	O. Time (UTC)	Lat. (N)	Log. (E)	RFD (km)	*M*	CFD (km)	M_W	Mo dyne-cm	Plane 1			Plane 2			Principal stress axes					
										S	*D*	*R*	*S*	*D*	*R*	*T*		*N*		*P*	
																PL	AZ	PL	AZ	PL	AZ
1	2005/01/25	16:44:09.9	37.54	43.78	10	5.4 m_b	16 ± 4	5.66	3.89e + 24	120	90	−175	030	85	000	04	255	85	120	04	345
2	2005/02/02	23:26:53.4	37.75	43.62	08	4.6 m_b	18 ± 4	4.11	1.84e + 22	312	71	−137	205	50	−025	13	074	44	331	43	176
3	2006/06/06	17:03:05.5	35.69	46.04	30	5.0 m_b	13 ± 3	4.21	2.60e + 22	102	58	116	240	40	055	66	062	22	268	10	174
4	2006/09/16	08:54:21.7	35.29	45.40	80	4.5 m_b	17 ± 5	3.92	9.55e + 21	080	65	035	334	59	150	42	299	48	111	04	205
5	2008/02/18	03:08:47.1	36.36	40.87	06	3.9 M_L	15 ± 6	3.51	2.32e + 21	320	85	−020	052	70	−175	10	007	69	127	18	274
6	2008/05/11	23:20:07.7	37.76	43.20	40	4.1 M_L	17 ± 5	3.89	8.61e + 21	070	75	−025	167	66	−164	06	120	61	221	28	027
7	2008/07/05	19:00:18.7	36.22	42.25	03	3.6 M_L	14 ± 4	3.22	8.51e + 20	218	86	−145	125	55	−005	21	346	55	224	27	087
8	2008/12/14	16:23:41.4	36.01	44.95	10	3.8 M_L	17 ± 5	3.70	4.47e + 21	163	77	−149	065	60	−015	11	291	57	183	31	028
9	2009/03/01	20:53:32.6	36.89	42.17	02	3.9 M_L	14 ± 4	3.63	3.51e + 21	268	80	129	010	40	015	41	215	38	081	25	329
10	2009/04/23	00:26:20.5	37.00	42.62	10	3.8 M_L	20 ± 6	3.62	3.39e + 21	160	80	−025	255	65	−169	10	209	63	320	25	115
11	2009/09/20	20:14:47.1	36.27	40.85	10	3.9 M_L	14 ± 4	3.59	3.05e + 21	054	76	−164	320	75	−015	00	187	69	096	21	277
12	2010/01/07	17:46:10.6	36.43	41.22	05	3.5 M_L	24 ± 6	3.32	1.20e + 21	330	65	055	209	42	141	55	194	31	346	13	085
13	2010/05/07	14:21:37.4	36.49	42.82	11	3.6 M_L	23 ± 5	3.46	1.95e + 21	234	72	−154	135	65	−020	05	003	58	266	31	096
14	2010/08/08	17:35:17.7	36.84	45.15	10	4.1 m_b	20 ± 6	3.34	1.29e + 21	275	70	−025	014	67	−158	02	325	58	059	32	234
15	2010/11/22	10:38:02.0	36.98	42.86	05	4.2 M_L	20 ± 7	4.01	1.30e + 22	067	81	160	160	70	010	21	022	68	223	07	115
16	2011/05/29	14:30:11.0	37.32	42.55	02	3.7 M_L	21 ± 5	3.24	9.12e + 20	185	75	−045	290	47	−159	17	243	43	350	42	137
17	2011/10/27	08:04:22.0	37.21	43.93	10	5.1 m_b	19 ± 3	4.69	1.36e + 23	215	90	070	125	20	180	42	106	20	215	42	324
18	2011/12/06	15:46:28.0	37.30	43.94	02	4.5 M_L	15 ± 4	4.15	2.11e + 22	139	81	−155	045	65	−010	11	270	63	158	24	005
19	2012/03/05	06:50:34.0	35.04	44.09	02	4.7 m_b	25 ± 6	4.83	2.21e + 23	145	70	080	352	22	116	64	039	09	148	24	243
20	2012/04/24	23:28:53.0	37.42	44.75	02	3.8 M_L	15 ± 4	3.77	5.69e + 21	306	76	−154	210	65	−015	08	076	61	332	28	170
21	2012/05/05	01:57:13.0	35.10	44.16	15	4.4 m_b	22 ± 5	4.76	1.74e + 23	186	87	110	285	20	010	45	115	20	004	38	258
22	2012/06/15	23:48:15.0	37.20	42.44	02	4.2 M_L	14 ± 4	4.22	2.69e + 22	210	80	−015	303	75	−170	03	257	72	357	18	166
23	2012/06/16	03:12:55.0	37.19	42.45	02	3.7 M_L	14 ± 4	3.50	2.24e + 21	035	80	025	300	65	169	25	260	63	055	10	166
24	2012/09/12	23:29:38.0	37.21	43.57	02	4.2 M_L	22 ± 7	4.14	2.04e + 22	163	82	−114	055	25	−020	33	273	23	167	48	48
25	2012/09/13	02:42:21.0	36.99	43.72	02	4.2 M_L	13 ± 5	4.39	4.84e + 22	060	85	−020	152	70	−175	10	108	69	227	18	014

O. Time (UTC) original time in UTC, *Lat* latitude in degree, *Log* longitude in degree, *RFD* reported focal depth, *M* reported magnitude, *CFD* calculated focal depth, M_W moment magnitude, *Mo* seismic moment measured in dyne-cm, *S* strike, *D* depth, *R* rake angle, *T, N, and P* tensional, normal, and compressional principal stress axes respectively

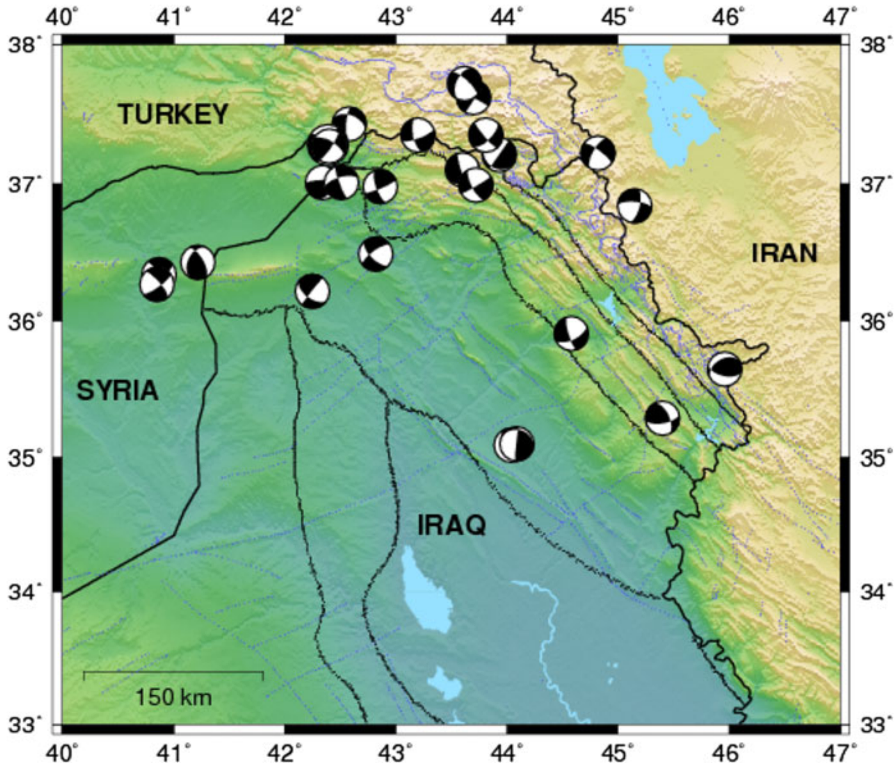

Figure 7
Moment tensor solutions for 25 earthquakes in the Bitlis–Zagros Fold and Thrust Belt in Iraq shown in a lower hemisphere equal-area projection

9.4. Depths

The depth distribution of earthquakes in the Zagros Mountains in Iran has been highly debated for many years. Early seismic studies reported earthquakes in the upper crust and upper mantle, but not in the lower crust (Bird *et al.* 1975; Nowroozi 1971). However, recent studies suggest that earthquakes occur only within the upper crust (Jackson and Fitch 1981; Maggi *et al.* 2000; Jackson 2002; Tatar *et al.* 2004). In general, depths of earthquakes in the Zagros Mountains have focal depths less than 30 km (Jackson 1980; Engdahl *et al.* 2006). Fahmi *et al.* (1986) reported that the strike-slip faulting occurs at shallow depths or crust as a result of an inequilibrium in the overlying rock masses with incumbent tensional forces, and reverse faulting or even thrust faulting occurring at basal crustal depths due to regional compressive stresses. However, Jackson and Fitch (1981) reported that the fault plane solutions for earthquakes below the simply folded belt in Iran show high angle thrust faulting with depth ranging from 8 to 15 km. Our results show that all of the 25 events have a focal depths ranging between 13 and 25 km, while the reported focal depths of 22 of these events according to the EMSC ranged between 2 and 15 km and the three other events are 30, 40, and 80 km (see Table 1).

10. Conclusion

According to our results, the moment tensor inversion for the 25 events predicted focal depths ranging from 13 to 25 km. That means these events occurred in the lower part of the upper crust and the upper part of the lower crust. Most of the earthquakes in the Bitlis trend region are concentrated between depths of 10–20 km with a strike-slip mechanism, while most of the earthquakes in the Zagros trend region occurred around focal depths ranging between

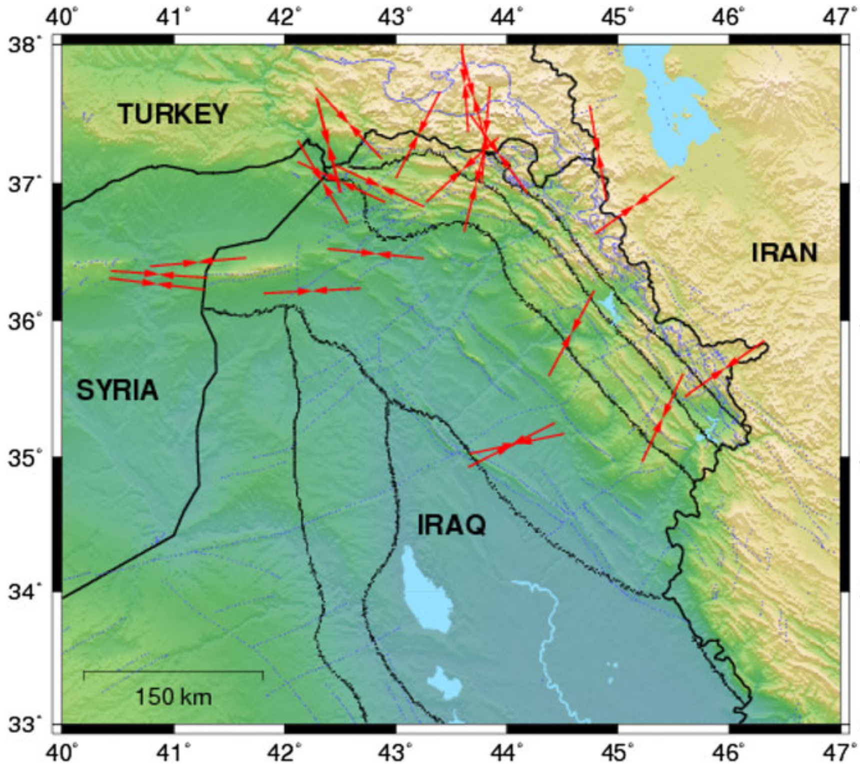

Figure 8
Stress vectors of compression (*P*) axes from moment tensor solutions for 25 earthquakes in the Bitlis–Zagros Fold and Thrust Belt in Iraq shown in a lower hemisphere equal-area projection

20 and 30 km and had reverse-slip mechanisms with slight strike-slip components. We envisage that reverse faulting in the Bitlis–Zagros Fold and Thrust Belt has occurred as a result of basement reactivation due to compressional stresses instigated by continental plate collision. In our view, this reverse displacement mechanism occurred on the inherited originally normal listric faults whose curved planes cut deep in the crystalline basement complex, hence the deep foci of the earthquakes with reverse-slip mechanisms. On the other hand, the earthquakes which were shown in this study to be due to strike-slip faults in the Bitlis Fold and Thrust Belt have shallower depths. Since these faults are associated with the overall tectonic lateral westward escape of Turkey along the two major East Anatolian and North Anatolian strike-slip faults, which are exposed at the surface and are due to the space problem arising from the collision of the Arabian and Turkish plates, this gives rise to shallower depth earthquakes.

The regional stress regime as evidenced from our analysis in the study area shows that the major compressional directions are: NNE-SSW and NW–SE in the Bitlis Fold and Thrust Belt, and NE-SW in the Zagros Fold and Thrust Belt. These major compressional stress directions are comparable with the stress regime in the area. In this paper, we have studied the general orientation of the stress regime. We are planning to analyze more data in order to determine the principal stress axes and identify the stress regimes in the area.

Acknowledgments

We thank Dr. Robert Herrmann for allowing us to use his software package and for his continuous and unlimited help; and Wessel and Smith for the GMT software. Also, we thank Albert Everett for his continuous involvement and help with the software installation and execution. Thanks go to IRIS, KOERI, and EMSC for the seismic data and catalog. Special thanks go to the Iraqi Seismological Network for providing some of the data for this research.

References

Abdulnaby, W., Mahdi, H., and Al-Shukri, H. (2012), Crustal structure from joint inversion of receiver function and surface wave dispersion beneath Duhok, NW Iraq, Istanbul International Geophysical Conference and Oil and Gas Exhibition, Istanbul, Turkey, 17–19 September 2012.

Afsari, N., Sodoudi, F., Taghizadeh, F., and Reza, G. M. (2011), *Crustal structure of Northwest Zagrs (Kermanshah) and Central Iran (Yazd and Isfahan) Using Teleseismic Ps Converted Phase*, Journal of Seismology, *15*, 341–353.

Al-Heety, E. A. (1997), *Fault plane solution of Harer Earthquake of 24 July 1991, North of Iraq*, Journal of Al-Anbar University, *1*, 125–128.

Alsinawi, S. A., and Al-Heety, E. A. (1997), *Composite Focal Mechanism of Microearthquake Parameters in North Central Iraq*, Jour. of Al Anbar University, *1*, 102–112.

Alsinawi, S. A., and Al-Heety, E. A. (1994), *Crustal Thickness Determination in Iraq from long-period P-wave spectra*, Iraqi Geol. J., *25*, 28–49.

Bird, P., Toksöz, M., and Sleep, N. (1975), *Thermal and mechanical models of continent-continent convergence zones*, Journal of Geophysical Research, B, Solid Earth and Planets, *80*, 4405–4416.

Dewey, J. F., Pitman, W. C., Ryan, W. B. F., and Bonnin, J. (1973), *Plate tectonics and evolution of the alpine system*, Bull. Geol. Soc. Am., *84*, 3137–3180.

Elitock, Ö, and Dolmaz, M. N. (2011), Tectonic Escape Mechanism in the crustal evolution of Eastern Anatolian Region (Turkey), In: New frontiers in tectonic research—at the midst of plate convergence (ed. Uri Schattner) (INTECH, 2011) pp. 289–302.

Engdahl, E. R., Jackson, J., Myers, S., Bergman, E., and Priestley, K. (2006), *Relocation and assessment of seismicity in the Iran Region*, Geophys. J. Int., *167*, 761–778.

Engelder, T. (1993), Stress regimes in the lithosphere, Princeton University Press, p. 457.

Fahmi, K. J., Al-Salim, M. A. H., and Ayar, B. S. (1986), *Recent earthquake activity in the lesser Zab Region of Northeastern Iraq*, Tectonophysics, *131*, 89–111.

Falcon, N. L. (1974), *Southern Iran: Zagros Mountains, in Mesozoic-Cenozoic Orogenic Belts: Data for orogenic studies: Alpine-Himalayan Orogens*, Geol. Soc. London Spec. Pub., *4*, 199–211.

Gök, R., Mahdi, H., Al-Shukri, H., and Rodgers, J. A. (2008), *Crustal Structure of Iraq from receiver functions and surface wave dispersion: implications for understanding the deformation history of the Arabian-Eurasian collision*, Geophysical Journal Int., *172*, 1179–1187.

Gök, R., Pasyanos, M., Zor, E. (2007), *Lithospheric structure of the continent–continent collision zone: Eastern Turkey*, Geophysical Journal International, *169*, 1079–1088.

Gök, R., Mellors, R.J, Sandvol, E., Pasyanos, M., Hauk, T., Takedatsu, R., Yetirmishli, G., Teoman, U., Turkelli, N., Godoladze, T., Javakishvirli, Z., (2011), *Lithospheric velocity structure of the Anatolian plateau–Caucasus–Caspian region*. Journal of Geophysical Research, *116*, p. B05303.

Gritto, R, Sibol, M. S., Siegel, J. E., Ghalib, H. A., Chen, Y., Herrmann, R. B., Alequabi, G. I., Tkalcic, H., Ali, B. S., Saleh, B. I., Mahmood, D. S., Shaswar, O. K., Mahmood, A., Abdullah, S., Ibrahim, F., Zand, R., Ali, B., Omar, L., Aziz, N. I., Ahmed, N. H., Al-Nasiri, T., Ali, A. A., Taqi, A. A., and Khalaf, S. R. (2008), Crustal structure of North Iraq from receiver function analysis. Unpublished report from monitoring research review: ground-based nuclear explosion monitoring technologies, Sponsored by Air Force Research Laboratory, p. 8.

Havskov, J., and Ottemöller, L. (2010), Routine data processing in earthquake seismology, Springer, p. 347.

Herrmann, R. B. (2006), An overview of synthetic seismogram computation, In: Computer programs in seismology, Version 3.30, Saint Louis University.

Herrmann, R. B., and Ammon, C. J. (2003), Source inversion, In: Computer programs in seismology, Version 3.30, Saint Louis University.

Herrmann, R. B., and Ammon, C. J. (2004), Computer programs in seismology, Version 3.30, Saint Louis University, Missouri.

Herrmann, R. B., Malagnini, Luca, and Munafò, Irene (2011), *Regional moment tensor of the 2009 L'Aqila Earthquake sequence*. Bulletin of the Seismological Society of America, *101*, 975–993.

Herrmann, R. B. (2011), Training course moment tensor inversion. In: Computer programs in seismology, Version 3.30, Saint Louis University.

Jackson, J. A. (1980), *Reactivation of Basement Faults and Crustal Shortening in Orogenic Belt*, Nature, *283*, 343–346.

Jackson, J. A. (2002), *Strength of the continental lithosphere: time to abandon the jelly sandwich?*, GSA Today, p. 9.

Jackson, J., and Fitch, T. (1981), *Basement faulting and the focal depths of the larger earthquakes in the Zagros Mountains (Iran)*, Geophysical Journal International, *64*, 561–586.

Kanamori, H. (1983), *Magnitude scale and quantification of earthquakes*, Tectonophysics, *93*, 185–199.

Kayal, J. R. (2008), Microearthquake seismology and seismotectonics of South Asia, Springer, p.503.

Kim, S. G., and Nuttli, O. W. (1977), *Spectral and magnitude characteristics of anomalous Eurasian earthquakes*, Bulletin of the Seismological Society of America, *67*, 463–478.

Maggi, A., Jackson, J., Priestley, K., and Baker, C. (2000), *A re-assessment of focal depth distributions in Southern Iran, the Tien Shan and Northern India: do earthquakes really occur in the continental mantle?*, International Journal of Geophysics, *143*, 629–661.

Mellors, R., Gök, R., Pasyanos, M., Skobeltsyn, G, Teoman, U, Godoladze, T., and Sandvol, E. (2008), High-resolution seismic velocity and attenuation models of the Caucasus-Caspian Region, LLNL-PROC-405214.

Mooney, W. D., Laske, G., and Masters, G. (1998), *CRUST 5.1: a global crustal model at 5° × 5°*, J. Geophys. Res., *103*, 727–747.

Nowroozi, A. A. (1971), *Seismotectonics of the Persian Plateau, Eastern Turkey, Caucasus, and Hindu-kush Regions*, Bulletin of the Seismological of America, *61*, 317–341.

Numan, N. M. S. (2001), *Cretaceous and tertiary Alpine subductional history in Northern Iraq*, Iraqi Jour. of Earth Sci., *1*, 59–74.

Numan, N. M. S. and Al-Azzawi, N. K. B. (1993), *Structural and geotectonic interpretation of vergence directions of anticlines in the foreland folds of Iraq*. Abhath Al-Yarmouk, *2*, 57–73.

Numan, N. M. S. (1984), *Basement controls of stratigraphic sequences and structural patterns in Iraq*, Geol. Soc. Iraq. Jour., *16*, 8–28.

Numan, N. M. S. (1997), *A plate tectonic scenario for the phanerozoic succession in Iraq*, Iraqi Geological Journal, *30*, 85–119.

Numan, N. M. S. (2000), *Major Cretaceous tectonic events in Iraq*, Raf. Journal Science, *11*, 3, 32–52.

Numan, N. M. S., Hammoudi, R.A., and Chorowicz, J. (1998), *Synsedimentary tectonics in the Eocene Pila Spi limestone formation in Iraq and its geodynamic implications*, Journal of African Earth Sciences, *27*, 141–148.

Sengor, A.M.C., Gorur, N., Saroglu, F. (1985), Strike-slip faulting and related basin formation in zones of tectonic escape: Turkey as a case study. In: Biddle, K.T. and Christie-Blick, N. (Eds.), Strike-slip deformation, basin formation and sedimentation. Society of Economic Mineralogist and Paleontologists Special Publication *37*, 227–264.

Shearer, P. M. (2009), Introduction to seismology, Cambridge, p. 396.

Stocklin, J. (1968), *Structural history and tectonics of Iran, a review*, Bull. A.A.P.G., *52*, 1229–1258.

Tatar, M., Hatzfeld, D., and Ghafori-Ashtiany, M. (2004), *Tectonics of the Central Zagros (Iran) deduced from microearthquake seismicity*, Geophysical Journal International, *156*, 255–266.

(Received February 5, 2013, accepted June 6, 2013)